Journal of Alloys and Compounds 513 (2012) 546–551

Contents lists available at SciVerse ScienceDirect

Journal of Alloys and Compounds

journal homepage: www.elsevier.com/locate/jallcom

Effect of cohesive energy on thermal expansion behavior of T6 tempered 7A09 aluminum alloy

Lin Yuan, Hongzhi Ji, Debin Shan*

School of Materials Science and Engineering, Harbin Institute of Technology, Harbin 150001, PR China

ARTICLE INFO

Article history:
Received 8 July 2011
Received in revised form 30 October 2011
Accepted 1 November 2011
Available online 9 November 2011

Keywords:
Aluminum alloy
Phase transition
Cohesive energy
Thermal expansion

ABSTRACT

The dynamic effect of cohesive energy on the CTE of T6 (the highest strength temper) tempered 7A09 aluminum alloy was studied in this paper. Transmission electron microscopy (TEM) was combined with differential scanning calorimetry (DSC) to analyze the phase transitions of T6 tempered 7A09 aluminum alloy taking place in a heating process. The corresponding CTE curve was recorded by a thermal dilatometer. The ion-bonding model was utilized to estimate the variation of cohesive energy caused by the phase transitions. Results indicate that GPII zones and η' phase are main precipitates in T6 tempered 7A09 alloy. During the heating process, the cohesive energy of alloy system increases with the transition from η' to η phase and the precipitation of η phase. The dissolution of η phase leads to a decrease of cohesive energy. Although volume changes of alloy system have effects on the CTE, the effect of the cohesive energy change is more obvious than that of volume change after the precipitation of η phase begins in the Ostwald ripening stage. Effects of cohesive energy and volume changes can be expressed in the nonlinearity of CTE curve.

1. Introduction

The thermal expansion is an important thermophysical property of materials, which can be quantitively described by the coefficient of thermal expansion (CTE). As for metals and alloys, the thermal expansion has critical implications for technologies that process these materials at elevated temperature [1]. The residual stress can be caused by the thermal heterogeneity of materials in the changing temperature process of different technologies such as casting, forging, rolling and so on [2–4]. The thermal heterogeneity mentioned above mainly refers to the heterogeneity of CTE, temperature field and so forth. The non-uniform thermal distortion and the thermal stress influence the product quality and do harm to material performances if they have not been properly controlled [4–7]. Therefore, the thermal expansion behavior of metals and alloys is a key issue for defect control, performance prediction and optimization of technologies.

The cohesive energy is a basic physical quantity used to characterize the strength of the chemical bond between atoms in solids. And it is closely related to the thermal expansion behavior of solids [8–12]. Crystals show thermal expansion when the amplitude of atoms and the space between atoms increase with the increasing temperature. As for crystals with the same temperature, the magnitude of thermal expansion depends on the cohesive energy level between atoms. The magnitude of thermal expansion is usually smaller for the crystal with higher cohesive energy. Tsuru et al. studied the relationship between the CTE and the cohesive energy according to substantive experimental data of linear thermal expansion coefficient. They suggested that the CTE was inversely proportional to the cohesive energy for various metals, oxides, borides, carbides and nitrides [10]. Jung et al. found that the CTE varied inversely as the melting temperature, which is generally proportional to the cohesive energy [13–15], for Half-Heusler compounds of MNiSn (M = Ti, Zr, Hf) [11]. As for alloys, the cohesive energy is also a key factor influencing CTE [12]. Effects of the cohesive energy change can be directly expressed in the nonlinearity of CTE curve.

7A09 alloy (a Chinese brand) is a kind of Al–Zn–Mg–Cu type aluminum alloy, which has been used for complex aeronautical applications due to its desirable mechanical properties. The isothermal forging is one of the main methods to process 7A09 aluminum alloy because the alloy has narrow forming temperature range and big heat conductivity coefficient. Furthermore, isothermal forgings usually have homogeneous microstructures and excellent properties [16,17], which are very important for aeronautical applications. The T6 temper state is the common initial state of the blank for the isothermal forging of 7A09 alloy.

Although many studies have been carried out to analyze the relationship between the cohesive energy and the thermal expansion, the dynamic effect of cohesive energy on the thermal

* Corresponding author. Tel.: +86 451 86418732; fax: +86 451 86418732.
E-mail address: shandb@hit.edu.cn (D. Shan).

0925-8388/$ – see front matter © 2011 Elsevier B.V. All rights reserved.
doi:10.1016/j.jallcom.2011.11.003

expansion behavior of aluminum alloy has seldom been studied and mentioned. Furthermore, the study on thermal expansion behavior of T6 tempered 7A09 alloy is necessary for the technology points such as the design of forging dies, the accuracy control of final forgings and so on. The present paper has dealt with the relationship between phase transitions, cohesive energy and CTE of the T6 tempered 7A09 aluminum alloy in a heating process. The DSC technique has been combined with TEM to characterize the microstructure evolution. The corresponding CTE curve of 7A09 aluminum alloy is recorded by a thermal dilatometer. The ion-bonding model [18,19] has been utilized to estimate the variation of cohesive energy caused by the phase transitions.

2. Experimental details

The results reported in this study refer to a commercial T6 tempered 7A09 alloy with the following chemical composition (wt%): 5.8 Zn, 2.8 Mg, 1.49 Cu, 0.23 Cr, 0.45 Fe, 0.063Si, 0.024 Ti, Bal. Al.

Precipitation and dissolution in the heating process were characterized by the DSC on a NETZSCH STA 449C instrument. Samples for DSC were polished into disks of 3 mm in diameter and 0.5 mm in thickness. They were heated at a rate of 5 °C/min from room temperature up to 470 °C. Dried nitrogen (30 ml/min) was passed through the calorimeter to minimize oxidation. The formation of AlN is a possible problem which may influence DSC data. The melt of aluminum is a necessary condition for the formation of AlN through the reaction between Al and N_2 while the melting-point of 7A09 alloy is about 640 °C. Therefore, the formation of AlN is not a main influence factor for the DSC analysis in present research when experiment temperature is lower than 470 °C. The TEM investigations included conventional bright-field, selected area electron diffraction (SAED), high resolution transmission electron microscopy (HRTEM) and numerical diffractogram analysis. Some samples were heated up to the specific temperature at a rate of 5 °C/min and quenched in water for the observation of high-temperature microstructure. TEM thin foils were polished mechanically to a thickness of 100 μm and then electropolished in a solution of 1/3 nitric acid and 2/3 methanol at −20 °C under an applied voltage of 15 V. The foils were observed by a TECNAI G2F30 high resolution transmission electron microscope (300 kV). The corresponding CTE curve was obtained on a NETZSCH DIL 402C instrument. Samples for the dilatometry were cut and polished into cubes with a length of 4 mm. Dried argon (50 ml/min) was used to protect samples from oxidation.

3. Results and discussion

3.1. Microstructure characterization

T6 temper is the peak-aged heat treatment for 7A09 alloy. It consists of the solution treatment at 470 ± 5 °C and the ageing for 16 h at 140 ± 5 °C. Fig. 1 shows the TEM micrograph of 7A09 alloy in the T6 temper state. It reveals that very fine precipitates distribute homogeneously inside grains with a few coarse precipitates

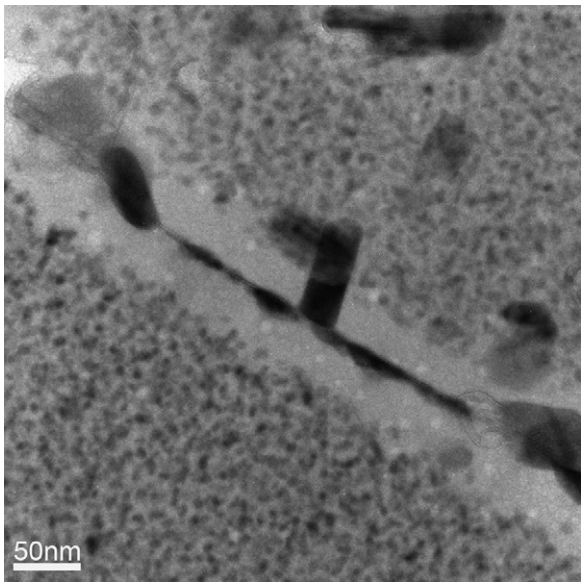

Fig. 1. TEM micrograph of 7A09 alloy in the T6 temper state.

appearing both on the grain boundaries and in the grain interiors. The coarse precipitates are likely to be η phase [20–22]. Fig. 2(a) shows the SAED pattern of fine intragranular precipitates in $[1\,1\,1]_{Al}$ projection. The diffraction spots of the aluminum matrix have been indexed, and the spots from η' phase and GPII zones can be identified according to the model reported in some published literatures [23,24]: spots belonging to η' phase appear around positions of $1/3\{2\,2\,0\}_{Al}$, $2/3\{2\,2\,0\}_{Al}$, and $1/3\{4\,2\,2\}_{Al}$ and spots arising from GPII zones can also be observed near the position of $1/3\ \{4\,2\,2\}_{Al}$, see the schematic pattern of Fig. 2(b). It can be found from Fig. 3(a), a HRTEM image, that the predominant fine precipitates in the grains are polygonal particles. And the numerical diffractogram shown in Fig. 3(b) indicates that the polygonal particle belongs to η' phase. The orientation relationship between the precipitate of η' phase and matrix is identified according to Fig. 3(b): $\{0\,0.1\}\eta//\{1\,1\,1\}_{Al}$ and $\{1\,0.0\}\eta//\{0\,1\,1\}_{Al}$.

The DSC result shown in Fig. 4 is obtained from the heating process of T6 tempered 7A09 alloy. It has an endothermic peak A (190 °C) and an endothermic region D (280–440 °C), as well as two exothermic peaks, B (225 °C) and C (251 °C). Generally, GP Zones of 7000 series aluminum alloys are relatively stable at the room

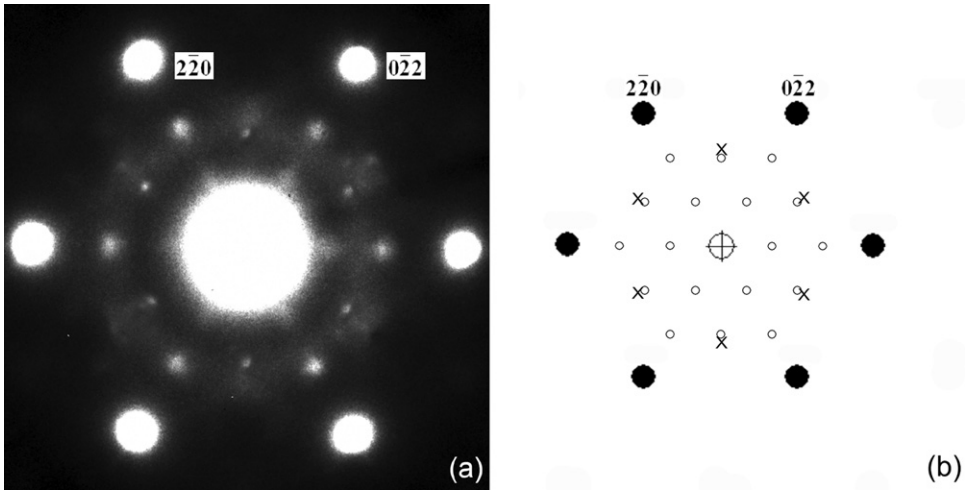

Fig. 2. SAED pattern of 7A09 alloy in the T6 temper state: (a) $[1\,1\,1]_{Al}$ projection, (b) schematic representation of $[1\,1\,1]_{Al}$: small open circles-η', cross-GP II zones.

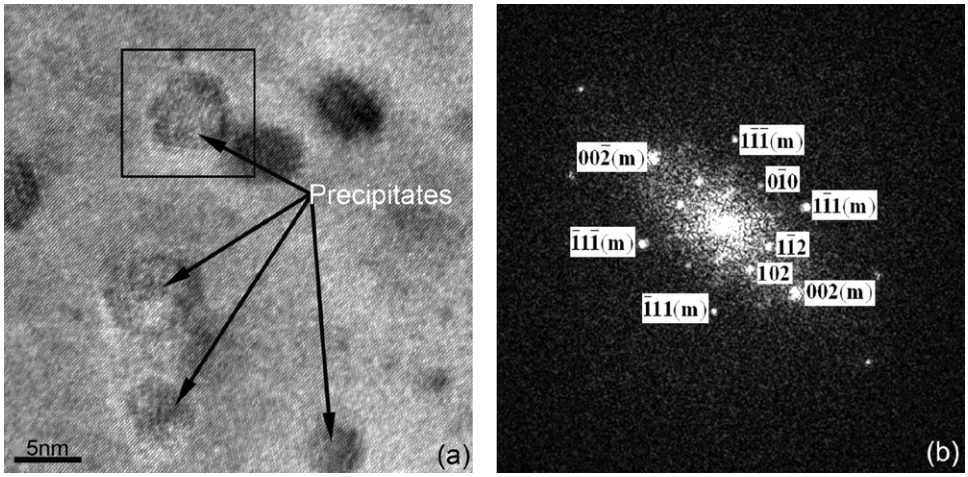

Fig. 3. HRTEM image of precipitates and associated numerical diffractogram: (a) HRTEM image, (b) numerical diffractogram of precipitate in the square zone attained along $[1\,1\,0]_{Al}$ direction ("m" refers to matrix).

temperature up to 120 °C [25]. Hence the endothermic peak A is mainly due to the dissolution of GP II Zones. After GP II Zones have dissolved in the matrix, η' phase has tendencies to dissolve and to transform into η phase with the increasing temperature [22,26]. TEM micrograph of 7A09 alloy and HRTEM image of fine precipitates at 225 °C have been shown in Figs. 5 and 6. In Fig. 5, it can be found that the density of precipitate does not show obvious changes. This means the dissolution of η' phase is not the main phase transition at 225 °C. In addition, the η phase has been found among fine precipitates as shown in Fig. 6(a). According to Fig. 6(b), the orientation relationship between this η precipitate and the matrix is confirmed: $\{0\,0\,.1\}\eta//\{1\,1\,0\}_{Al}$ and $\{1\,0\,.0\}\eta//\{0\,0\,1\}_{Al}$. The η particle observed in Fig. 6(a) belongs to η_1 phase [22,27]. Therefore, the exothermic peak B is the result of the transition from η' to η phase and the dissolution of η' phase. And the transition from η' to η is the main phase transition at 225 °C. The TEM micrographs of 7A09 alloy at 251 °C and 385 °C have been shown in Fig. 7(a and b) respectively. In Fig. 7(a), the precipitate is exclusively η phase [22,26]. The lager precipitate size and lower particle density than present at 225 °C suggest Ostwald ripening of the η precipitate [26]. The particle density shown in Fig. 7(b) is lower than that shown in Fig. 7(a), which means η phase dissolves into matrix again. Therefore, the final high temperature endothermic region D is mainly due to the solution of η phase.

3.2. Discussion about CTE variation of T6 tempered 7A09 alloy

The CTE curves of pure aluminum and 7A09 alloy have been shown in Fig. 8. As for pure aluminum, there are no phase transitions in the heating process and CTE changes linearly with the variation of temperature when temperature is higher than 80 °C [28]. There is a nonlinear dependency between CTE of 7A09 alloy and temperature as shown in Fig. 8. There are three obvious pivotal points (E, F, and G) on the CTE curve of 7A09 alloy. Temperature at point E, F and G are about 225, 330 and 425 °C, respectively. There is a nearly linear dependency between CTE and temperature in the range from 100 to 225 °C. The CTE curve deviates from linearity in the temperature range from E to G. The CTE increases with the increasing temperature linearly again when temperature is higher than 425 °C. Complex changes of the CTE curve have a close correlation with multiple phase transitions happening in the heating process. Cohesive energy and volume changes of alloy system caused by phase transitions are two main factors that may influence the variation trend of CTE.

Zn, Mg and Cu are main additional elements for 7A09 alloy. Atomic diameters of Al, Zn, Mg and Cu are 0.286 nm, 0.278 nm,

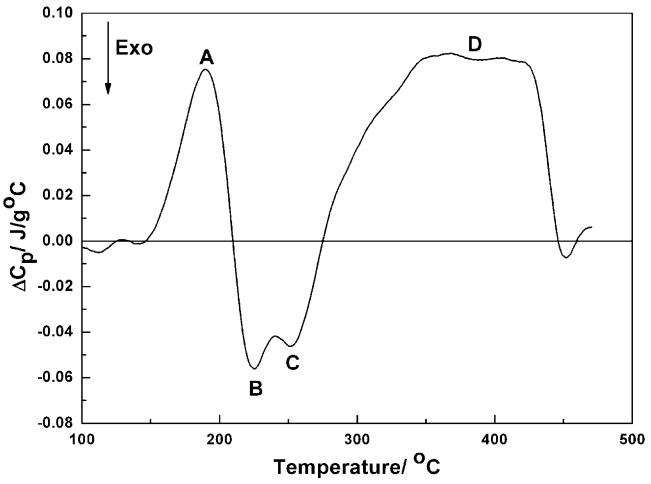

Fig. 4. DSC results obtained from the heating process of T6 tempered 7A09 alloy.

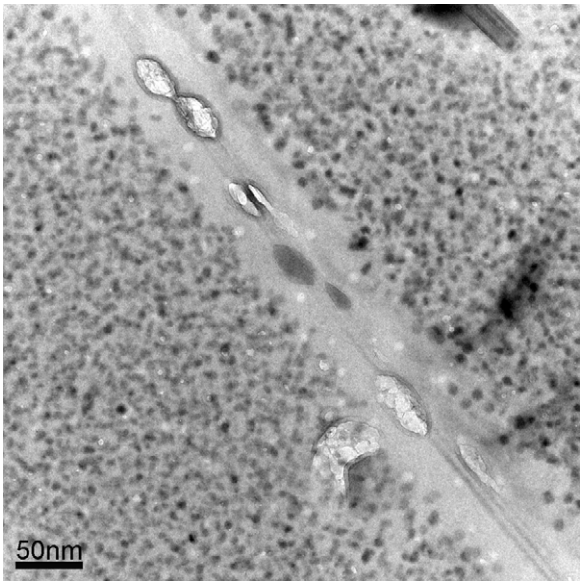

Fig. 5. TEM micrograph of the T6 tempered 7A09 alloy at 225 °C.

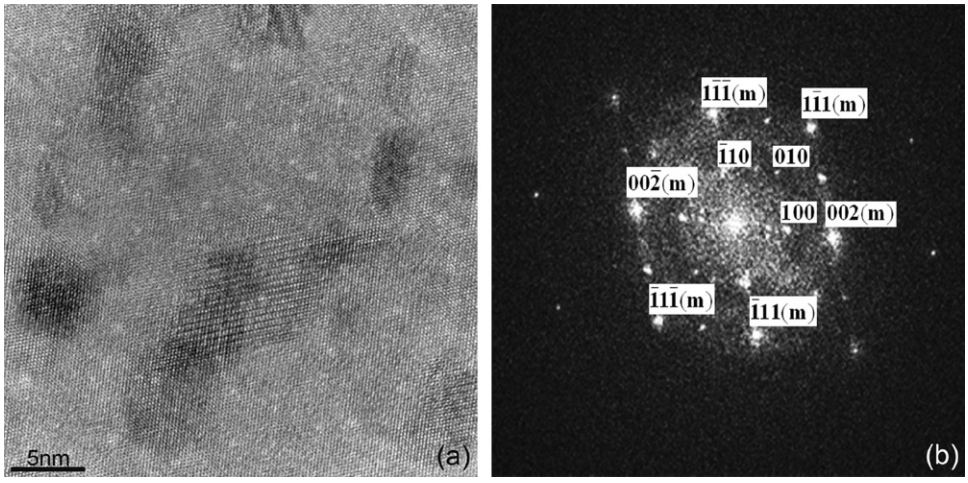

Fig. 6. HRTEM image of precipitates and associated numerical diffractogram at 225 °C: (a) HRTEM image, (b) associated numerical diffractogram of η phase obtained along $[1\,1\,0]_{Al}$ direction ("m" refers to matrix).

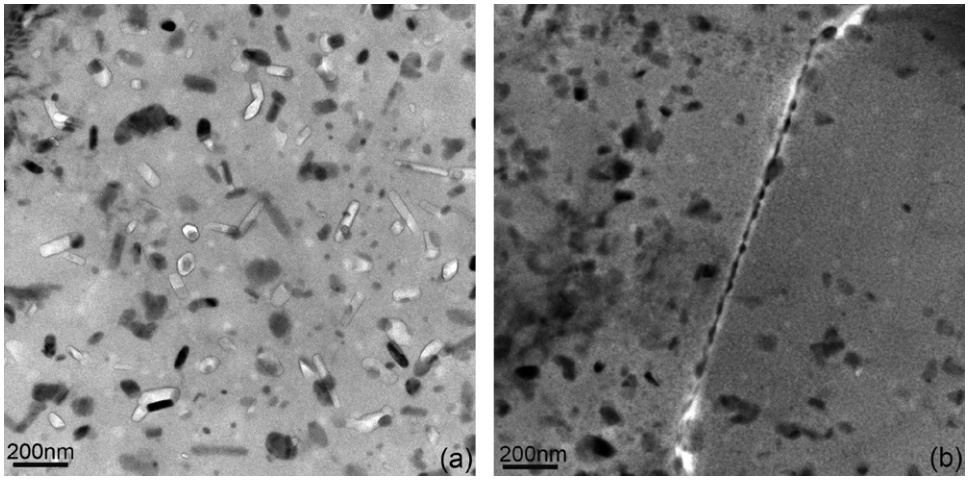

Fig. 7. TEM micrographs of the T6 tempered 7A09 alloy at 251 °C and 385 °C: (a) 251 °C, (b) 385 °C.

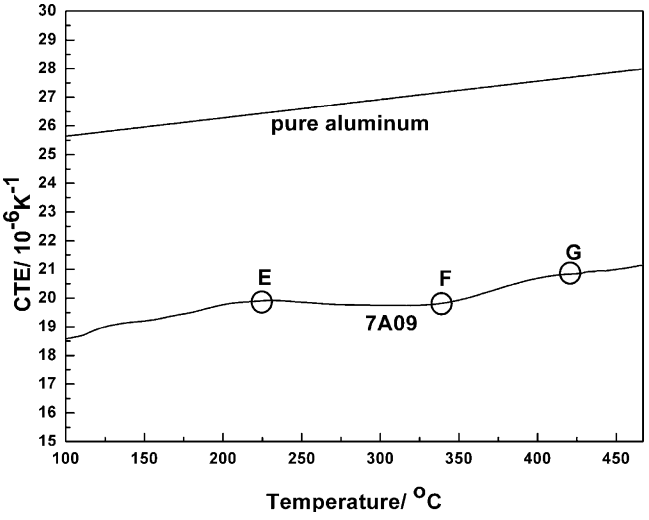

Fig. 8. CTE curves of pure aluminum and T6 tempered 7A09 alloy.

0.32 nm and 0.256 nm respectively [8]. Differences in atomic diameters are all less than 15% between Zn, Mg, Cu and Al. Moreover, the difference in the Gordy's scale of electronegativity is more than 0.4 only between Cu and Al. According to Hume-Rothery rule, substitution solid solution can be formed if Zn, Mg and Cu dissolve in aluminum matrix but the solubility of Cu in aluminum is very small. Consequently solution and precipitation of second-phase are mainly related to elements of Zn and Mg for 7A09 alloy.

Solid solutions of Al–Mg, Al–Zn and Al–Mg–Zn may be formed when Zn and Mg dissolve in the aluminum matrix. The structure type of these solid solutions is face-centered cubic [29]. In view of Mg and Zn content, lattice parameter of these solid solutions is about 0.41 nm and unit cell volume is about 0.06892 nm^3. The unit cell volumes of η phase and η' phase are about 0.202 nm^3 (lattice parameters of η phase: $a = 0.521$ nm, $c = 0.86$ nm) and 0.299 nm^3 (lattice parameters of η' phase: $a = 0.496$ nm, $c = 1.403$ nm). Consequently, the phase transitions will bring additional changes of alloy volume besides thermal volume changes during the heating process.

The change of cohesive energy arising from the phase transition is another possible factor which can influence the CTE of the alloy. Main changes of cohesive energy originate from a series of transitions such as the transition from η' to η phase as well as the precipitation and the dissolution of η phase. The cohesive enthalpy of precipitate can be calculated by [13,30]

$$\Delta H^{\text{form}}(1 \text{ mol of atoms}) = H^{\text{coh}} - C_A H_A^{\text{coh}} - C_B H_B^{\text{coh}} \quad (1)$$

where H^{coh} is the cohesive enthalpy of precipitate, H_A^{coh} and H_B^{coh} are the cohesive enthalpy of element A and B, C_A and C_B are the

Table 1
Parameters of ion-bonding model.

Element	E	F
Mg	0.03	2.30
Zn	5.31	0.00

atomic concentration of element A and B, ΔH^{form} is the formation enthalpy of precipitate. According to ion-bonding model, the formation enthalpy ΔH^{form} (cal/mol) of a specified type intermetallic compound can be described by

$$-\Delta H^{\text{form}} = C_A E_A + C_B E_B + \frac{1}{2} F_A F_B \quad (2)$$

where E_A, E_B, F_A, F_B are parameters based on experiment data. Parameters used in the calculation are shown in Table 1. Furthermore, it is noteworthy that ion-bonding model utilized in the calculation of the formation enthalpy is suitable for the binary intermetallic compound without aluminum.

According to the calculation based on ion-bonding model, the cohesive energy of η' phase and η phase are 148.68 and 149.86 kJ/mol respectively. As for η phase, the calculation result of cohesive energy is similar to the experiment result (142.5 kJ/mol) reported in the published literature [31]. The calculation result of the cohesive energy of η' phase has not been verified by the experiment result. But the melting-point of η' phase (about 347 °C) is lower than that of η phase (about 589 °C) [32], which indirectly implicates that the cohesive energy of η' phase is lower than that of η phase. Therefore, the cohesive energy of alloy system will increase when η' phase transforms into η phase. Furthermore, the cohesive energy of aluminum alloy will decrease with the increasing solute contents of Zn or Mg at temperature higher than room temperature [33]. Therefore, the dissolution of η phase can lead to a decrease of cohesive energy. On the contrary, the precipitation of η phase can lead to an increase of cohesive energy.

As has been noted, GPII Zones will dissolve in matrix when temperature is higher than 120 °C. But only little additional volume and cohesive energy changes can be formed with this phase transition because there are small amounts of GPII Zones in T6 tempered 7A09 alloy. Therefore, there is an approximate linear dependency between CTE and temperature in the range from 100 to 225 °C.

In the temperature range from E to G, multiple phase transitions may occur such as dissolution of η' phase, transition from η' to η phase, precipitation of η phase in the Ostwald ripening stage and dissolution of η phase. Thereinto, the latter three are the main phase transitions. The cohesive energy of alloy system will increase with the transition from η' to η phase and the precipitation of η phase, which can slow down the increase of CTE. The cohesive energy will decrease when the η phase dissolves in the matrix, which can accelerate the increase of CTE. The CTE decreases with the increasing temperature in the temperature range from E to F when the effect of energy is beneficial for slowing down the increase of CTE. The CTE increases with the increasing temperature again in the range from F to G when the cohesive energy change is good for accelerating the increase of CTE. After that the dependency between CTE and temperature is close to linearity again for the termination of phase transition. Therefore, there is a corresponding relation between the change of cohesive energy and the variation trend of CTE.

As for 7A09 alloy, an obvious additional contraction of alloy volume can be caused by the transition from η' to η phase and the dissolution of η phase during the heating process. The contraction can slow down the increase of CTE. The precipitation of η phase can lead to an additional increase of alloy volume, which can accelerate the increase of CTE. Obvious relationship between the variation of CTE and the volume changes will no longer exist after the precipitation of η phase begins in the Ostwald ripening stage. The incoherence between the η phase and the matrix is the main reason for this phenomenon. The incoherence heavily weakens the effect of the volume changes. Therefore, the effect of the cohesive energy is more obvious than that of volume change for the CTE of 7A09 alloy after the precipitation of η phase begins in the Ostwald ripening stage.

4. Conclusions

The dynamic relationship between phase transitions, the cohesive energy and CTE of 7A09 aluminum alloy (T6) in the heating process has been investigated by complementary experiments. The main results can be summarized as follows:

1. Cohesive energy and volume changes of alloy system caused by phase transitions influence the variation trend of CTE. And these effects can be expressed in the nonlinearity of CTE curve. After the precipitation of η phase begins in the Ostwald ripening stage, the effect of the cohesive energy change is more obvious than that of volume change for the CTE of 7A09 alloy.
2. According to the ion-bonding model, the cohesive energy of η' and η phase are 148.68 and 149.86 kJ/mol, respectively. The cohesive energy of alloy system increases with the phase transition from η' to η phase and the precipitation of η phase. The dissolution of η phase leads to a decrease of cohesive energy.
3. GPII zones and η' phase are main precipitates in T6 tempered 7A09 alloy. With the increasing temperature, obvious additional contraction of alloy volume is directly caused by phase transitions, such as dissolution of η' phase, transition from η' to η phase and dissolution of η phase. On the contrary, the precipitation of η phase leads to an additional increase of alloy volume.

Acknowledgements

The authors give thanks to National Natural Science Foundation of China (no. 50775051) and Youth Technology Speciality Fund of Harbin (no. 2008RFQXG052) for their financial support.

References

[1] J.D. James, J.A. Spittle, S.G.R. Brown, R.W. Evans, Meas. Sci. Technol. 12 (2001) R1–R15.
[2] M.M. Pariona, J.K. Rugenski, M.V. Canté, J.E. Spinelli, A. Garcia, Finite Elem. Anal. Des. 46 (2010) 889–895.
[3] V.G. Navas, O. Gonzalo, I. Quintana, T. Pirling, Mater. Sci. Eng. A: Struct. 528 (2011) 5146–5157.
[4] D. Gloaguen, M. François, R. Guillen, J. Royer, Acta Mater. 50 (2002) 871–880.
[5] S. Bruschi, A. Ghiotti, Int. J. Mach. Tool Manuf. 48 (2008) 761–767.
[6] J. Guan, G.W. Dieckhues, P.R. Sahm, Intermetallics 2 (1994) 89–94.
[7] C.-L. Chen, R.C. Thomson, Intermetallics 18 (2010) 1750–1757.
[8] C. Kittel, Introduction to Solid State Physics, 8th ed., John Wiley & Sons, Inc., New York, 2005.
[9] M. Xu, W.L. Gao, H.J. Zhang, X.F. Cheng, X.G. Xu, J.Y. Wang, R.I. Boughton, J. Alloys Compd. 509 (2011) 8455–8459.
[10] Y. Tsuru, Y. Shinzato, Y. Saito, M. Shimazu, M. Shiono, M. Morinaga, J. Ceram. Soc. Jpn. 118 (2010) 241–245.
[11] D.Y. Jung, K. Kurosaki, C.E. Kim, H. Muta, S. Yamanaka, J. Alloys Compd. 489 (2010) 328–331.
[12] R. Wang, Physical Properties of Metals, Metallurgical Industry Press, Beijing, 1985.
[13] F. Guinea, J.H. Rose, J.R. Smith, J. Ferrante, Appl. Phys. Lett. 44 (1984) 53–55.
[14] K.K. Nanda, S.N. Sahu, S.N. Behera, Phys. Rev. A 66 (2002), 013208-1-013208-8.
[15] C.H. Li, J.L. Hoe, P. Wu, J. Phys. Chem. Solids 64 (2003) 201–212.
[16] R. Kopp, J. Mater. Process. Technol. 60 (1996) 1–9.
[17] Y.Q. Zhang, D.B. Shan, F.C. Xu, J. Mater. Process. Technol. 209 (2009) 745–753.
[18] Z.Y. Qiao, Z.H. Xu, H.L. Liu, Computerized Physical Chemistry of Metallurgy and Materials, Metallury, Beijing, 1999.
[19] D.G. Zhao, P.M. Guo, P. Zhao, J. CSU, Sci. Technol. 42 (2011) 1578–1583.
[20] S.D. Liu, W.J. Liu, Y. Zhang, X.M. Zhang, Y.L. Deng, J. Alloys Compd. 507 (2010) 53–61.
[21] D. Godard, P. Archambault, E. Aeby-Gautier, G. Lapasset, Acta Mater. 50 (2002) 2319–2329.
[22] F. Viana, A.M.P. Pinto, H.M.C. Santos, A.B. Lopes, J. Mater. Process. Technol. 92–93 (1999) 54–59.

[23] L.K. Berg, J. Gjønnes, V. Hansen, X.Z. Li, M. Knutson-Wedel, G. Waterloo, D. Schryvers, L.R. Wallenberg, Acta Mater. 49 (2001) 3443–3451.
[24] Z.H. Li, B.Q. Xiong, Y.A. Zhang, B.H. Zhu, F. Wang, H.W. Liu, Mater. Charact. 59 (2008) 278–282.
[25] J. Lendvai, Mater. Sci. Forum 43 (1996) 217–222.
[26] R. Deiasi, P.N. Adler, Metall. Trans. 8 A (1977) 1177–1183.
[27] J.K. Park, A.J. Ardell, Metall. Trans. A 14A (1983) 1957–1965.
[28] M. Hu, F. Zheng, W.D. Fei, L.D. Wang, Z.K. Yao, Acta Mater. Compos. Sinica 19 (2002) 57–61.
[29] Y.J. Han, S.L. Chang, Y.J. Gao, Nonferr. Metal 59 (2007) 18–21.
[30] M.M. Wu, Y. Jiang, J.W. Wang, J. Wu, B.Y. Tang, L.M. Peng, W.J. Ding, J. Alloys Compd. 509 (2011) 2885–2890.
[31] M. Binnewies, E. Mike, Thermochemical Data of Elements and Compounds, Wiley/VCH, Toronto, 1999.
[32] T.B. Massalski, H. Okamoto, Binary Alloy Phase Diagrams, 2nd ed., ASM International, Metals Park, Ohio, 1994.
[33] S. Yamamoto, Acta Mater. 45 (1997) 3825–3833.